AIAA JOURNAL
Vol. 30, No. 7, July 1992

Standing Acoustic Waves in a Low Mach Number Shear Flow

Meng Wang* and David R. Kassoy†
University of Colorado, Boulder, Colorado 80309

Acoustic shear flow interactions are studied in a rectangular cavity bounded by impermeable duct walls parallel to the flow direction and special perpendicular acoustic reflectors that permit the passage of a fully developed, low Mach number shear flow. Fourier-series-based asymptotic solutions are constructed to provide an explicit description of the evolution of an initially imposed axial standing wave disturbance. The bulk convective motion of the shear flow is shown to be responsible for periodic axial waveform deformations. Additionally, transverse and oblique standing acoustic waves as well as single-frequency bulk oscillations arise from the refraction of the imposed axial acoustic disturbance by the mean flow velocity gradient. Combinations of these disturbances give rise to irregular acoustic pressure signals in the duct. Certain refraction induced transverse and oblique acoustic modes are amplified under resonant conditions. It is shown that, in the parameter ranges of solid rocket engines, the refraction and bulk convection effects are small, in general.

I. Introduction

THIS work describes the spontaneous evolution of a spatially distributed small initial disturbance imposed on a low Mach number shear flow in a duct. An initial boundary-value formulation is used to predict the complete spectrum of standing wave modes (or equivalently, combinations of traveling waves) generated by the interaction between the initial disturbance and the shear flow in a finite rectangular region. The primary objectives of this study are to demonstrate that 1) refraction of an axial wave arising from the relaxation of the initial disturbance is the source of a myriad of higher order (smaller) transverse and oblique acoustic waves, and 2) resonance conditions promote the amplification of a small subset of refraction induced transverse and oblique wave modes.

Traditional studies of acoustic shear flow interaction[1-3] examine the quasisteady properties of a sound wave, of the form $p = F(y)e^{i(\kappa x - t)}$, propagating in fully developed shear flows above a flat surface or in a planar duct. Linearization techniques are used to derive the fundamental equation governing the cross-stream eigenfunction F and the propagation constant κ. Asymptotic solutions[1,3] and numerical solutions[2,3] predict significant distortion of specific propagating wave modes as a result of acoustic refraction. When the wave is purely axial (the fundamental mode), the refraction effect is reflected in the variation of $F(y)$ across the shear flowfield.

In contrast to the quasisteady linear approach used in Refs. 1-3, Baum and Levine[4] used numerical methods to solve an initial boundary-value problem based on the Reynolds-averaged Navier-Stokes equations and the k-ϵ turbulence model. Their work is aimed at understanding mechanisms for energy exchange between the acoustic and mean flowfields in solid propellant rocket engines. In the model problem discussed in Ref. 4, an initially steady shear flowfield in a rigid walled axisymmetric cylinder is disturbed continuously at an inlet or outlet plane to generate unidirectional traveling acoustic waves. The waves move only a few acoustic wavelengths before computations are terminated, so that the quasisteady solution in Refs. 1-3 is not attained on the short time scale involved.

More recently, Wang and Kassoy[5] used an initial boundary-value approach to consider the two-dimensional planar duct counterpart of the refraction problem studied in Ref. 4. A systematic perturbation procedure based on the small mean flow Mach number M is used to demonstrate that nonlinear effects are $\mathcal{O}(M)$ smaller than the refractive contribution to the total acoustic pressure. The Fourier-series-based solution in Ref. 5 describes short-time acoustic transients arising from axial wave interaction with the shear flow, as well as their evolution into long-time quasisteady forms. In the nonresonant case, the solution includes not only the usual axial propagating mode, but also a finite number of oblique propagating modes, and an infinite number of nonpropagating bulk modes that decay rapidly away from the plane acoustic source. When resonance is present, a pair of amplified, trapped transverse waves also appear. The distinct modes have not been extracted from the numerical computations in Ref. 4.

It is of interest to extend the aforementioned traveling wave models of acoustic shear flow interaction to axially confined geometries in which multiple wave reflections occur. This is done in the present work by considering standing waves trapped between two wave reflectors separated by a finite axial distance in the duct examined in Ref. 5. The idealized model is used as a paradigm to demonstrate the surprisingly complex response of an initially steady shear flow to an imposed axial velocity disturbance in the confined region and to infer the acoustic convection and refraction magnitudes in solid rocket engine chambers. The inclusion of axial wave reflection effects in this study provides improved relevance to rocket engine acoustics, in comparison with the previous traveling wave studies.

Fourier-series-based analytical solutions give explicit modal response that may not be easily extracted from numerical data. The initial disturbance generates a leading-order acoustic field that is purely axial. It interacts with the shear flow to generate $\mathcal{O}(M)$ acoustic disturbances consisting of purely axial standing waves, transverse standing waves, oblique standing waves, and bulk fluid oscillations (Helmholtz modes). The linear combination of these disturbances gives surprisingly irregular $\mathcal{O}(M)$ pressure signals at a given location that could be mistakenly identified as a chaotic or turbulent response. The ratio of initial disturbance wavelength to duct width and the relationship between the disturbance and resonant frequencies are found to be important factors affecting the refraction magnitude, which is, in general, small except under resonant conditions. When resonance is present, amplifying modes exist, which can be represented as pairs of transverse and/or oblique traveling waves with growing amplitudes. The results of the present analysis are employed to show that, in

Received Jan. 22, 1991; revision received Sept. 12, 1991; accepted for publication Oct. 2, 1991.

*Research Associate, Center for Combustion Research, Department of Mechanical Engineering.

†Professor, Center for Combustion Research, Department of Mechanical Engineering.

the parameter ranges of typical solid rocket engine gasdynamics, refraction effects can produce only $\mathcal{O}(10\%)$ variations in acoustic pressure.

II. Mathematical Formulation

The conceptual model of the present acoustic shear flow interaction study is schematically illustrated in Fig. 1. A fully developed shear flow sweeps through a parallel duct region of length L', confined by rigid, impermeable sidewalls at $y' = \pm d'$. The thermodynamic state of the steady flowfield is defined by (p_0', ρ_0', T_0'), and the equilibrium speed of sound $c_0' = \sqrt{\gamma R T_0'}$, where R is the gas constant and γ the ratio of the specific heats.

An axially distributed, y'-independent initial disturbance to the steady flowfield evolves into transient acoustic oscillations on the acoustic time scale $t_a' = L'/c_0'$, which is much shorter than the mean flow passage time because the maximum mean flow Mach number, $M = U'_{\max}/c_0'$, is assumed to be small. Axial velocity components on the left and right boundaries of the flow configuration are assumed to be strictly equal to the shear flow velocity $U'(y')$. In other words, $x' = 0$ and $x' = L'$ represent fixed nodal surfaces for the axial acoustic velocity. This configuration is highly idealized, but provides an opportunity to develop an analytical investigation of trapped acoustic signals in shear flow when multiple wave refections occur on the axial boundaries.

The dimensionless equations for the compressible, viscous, and heat-conducting fluid motion in the duct are similar to those in Ref. 5,

$$p = \rho T \tag{1}$$

$$\rho_t + M[(\rho u)_x + (\rho v)_y] = 0 \tag{2}$$

$$\rho[u_t + M(uu_x + vu_y)] = -\frac{1}{\gamma M} p_x + \frac{M}{hR_e}\left(u_{yy} + \frac{4}{3}h^2 u_{xx} + \frac{1}{3}h^2 v_{xy}\right) \tag{3}$$

$$\rho[v_t + M(uv_x + vv_y)] = -\frac{1}{\gamma M h^2} p_y + \frac{M}{hR_e}\left(h^2 v_{xx} + \frac{4}{3}v_{yy} + \frac{1}{3}u_{xy}\right) \tag{4}$$

$$\rho[T_t + M(uT_x + vT_y)] = -M(\gamma - 1)p(u_x + v_y) + \frac{M}{hR_e}\frac{\gamma}{P_r}(T_{yy} + h^2 T_{xx}) + \frac{M^3}{hR_e}\Phi \tag{5}$$

where the thermophysical properties have been assumed constant for convenience. Subscripts t, x, and y denote partial derivatives; $R_e = U'_{\max} d'/\nu'$ is the mean flow Reynolds number; $h = d'/L'$ the aspect ratio of the duct; P_r the Prandtl number; and Φ the nondimensional dissipation function. Other nondimensional variables are defined in terms of dimensional quantities by

$$(p, \rho, T) = \frac{(p', \rho', T')}{(p_0', \rho_0', T_0')}, \qquad u = \frac{u'}{U'_{\max}}, \qquad v = \frac{v'}{hU'_{\max}}$$

$$x = \frac{x'}{L'}, \qquad y = \frac{y'}{d'}, \qquad t = \frac{t'}{t_a'} \tag{6}$$

The subsequent analysis is performed in the parameter ranges relevant to flow conditions in solid rocket engine chambers (excluding the exit nozzle), where the values of M and R_e are of $\mathcal{O}(10^{-1})$ and $\mathcal{O}(10^6)$, respectively.[6] Accordingly, it is reasonable to define the perturbation limit as $1/R_e \to 0$, $M \to 0$, and $1/R_e \ll M$. In addition, one assumes that the aspect ratio $h \leq \mathcal{O}(1)$.

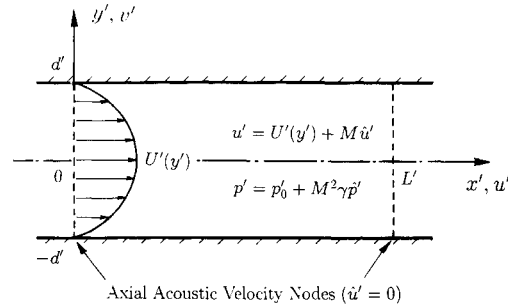

Fig. 1 Schematic of a parallel shear flow through a planar duct section containing acoustic disturbances.

Given the steady, fully developed shear flow velocities $u = U(y)$ and $v = 0$, one observes from Eqs. (1-5) that the basic pressure distribution is independent of the y direction, and that $dp/dx = \mathcal{O}(M^2/hR_e)$, negligible compared to the $\mathcal{O}(M^2)$ acoustic pressure to be considered. The high Reynolds number limit implies that viscous and thermal diffusion exerts little influence on the fluid motion, except in the thin acoustic boundary layers adjacent to solid surfaces, typically of thickness less than 1% of the duct width.[5] In this respect, the isentropic relations,

$$p = \rho^\gamma + \mathcal{O}\left(\frac{M}{hR_e}\right), \qquad T = \rho^{\gamma-1} + \mathcal{O}\left(\frac{M}{hR_e}\right) \tag{7}$$

together with the transport-free version of Eqs. (2-4) (the Euler equations) adequately describe the fundamental physical phenomena in the core flow region.

The traveling wave study in Ref. 5 is based on acoustic velocity disturbances of $\mathcal{O}(M)$ relative to the shear flow velocity $U(y)$. The corresponding acoustic thermodynamic disturbances muct be $\mathcal{O}(M^2)$, a magnitude frequently encountered in stable solid rocket motors, where an absolute pressure oscillation of 1-2% is often observed. When acoustic perturbations of the type

$$u = U(y) + M\hat{u}, \qquad v = M\hat{v} \tag{8}$$

$$p = 1 + M^2\gamma\hat{p}, \qquad \rho = 1 + M^2\hat{\rho}, \qquad T = 1 + M^2\hat{T} \tag{9}$$

are used in the transport-free version of Eqs. (2-4), the following equations are obtained for the acoustic variables:

$$\hat{\rho}_t + \hat{u}_x + \hat{v}_y + MU(y)\hat{\rho}_x + M^2[(\hat{\rho}\hat{u})_x + (\hat{\rho}\hat{v})_y] = 0 \tag{10}$$

$$\hat{u}_t + M[U(y)\hat{u}_x + \hat{v}U'(y)] + M^2(\hat{u}\hat{u}_x + \hat{v}\hat{u}_y) = -\frac{\hat{p}_x}{1 + M^2\hat{\rho}} \tag{11}$$

$$\hat{v}_t + MU(y)\hat{v}_x + M^2(\hat{u}\hat{v}_x + \hat{v}\hat{v}_y) = -\frac{\hat{p}_y}{h^2[1 + M^2\hat{\rho}]} \tag{12}$$

Equations (10-12) show that the mean flow $U(y)$ affects only the $\mathcal{O}(M)$ acoustic phenomena in the duct. The quadratic convective terms, representing the nonlinear effect in the wave system, are even smaller, of $\mathcal{O}(M^2)$.

The wave field evolves from an initial axially distributed velocity disturbance;

$$t = 0, \qquad \hat{u} = A\sin(k\pi x), \qquad \hat{v} = \hat{p} = 0 \tag{13}$$

Since the left and right boundaries are fixed nodal surfaces for $\hat{u}$,

$$x = 0,1 \qquad \hat{u} = 0 \tag{14}$$

The normal velocity component vanishes on the impermeable duct sidewalls. For mean flow $U(y)$ symmetric with respect to

the center plane ($y = 0$), the problem is symmetric and can be solved in the region $0 \le y \le 1$ only. The appropriate y boundary conditions are

$$y = 0,1 \qquad \hat{v} = 0 \tag{15}$$

III. Solution Development

The solution to the lowest order approximation to Eqs. (10–15) can be written as

$$p_1 = -A \sin(k\pi t)\cos(k\pi x) \tag{16}$$

$$u_1 = A \cos(k\pi t)\sin(k\pi x) \tag{17}$$

$$v_1 = 0 \tag{18}$$

where p_1, u_1, and v_1 are defined by the asymptotic expansions

$$\hat{\Psi} = \Psi_1 + M\Psi_2 + \mathcal{O}(M^2), \qquad \Psi = (u, v, p, \rho, T) \tag{19}$$

Note that for convenience the caret above Ψ_1 and Ψ_2 has been dropped. It follows from the isentropic relations (7), (9), and (19) that

$$p_1 = \rho_1, \qquad p_2 = \rho_2 \tag{20}$$

The leading-order solution in Eqs. (16–18) describes an axial mode with a harmonically time-varying amplitude, independent of the mean flow. In order to obtain information about how the shear flow affects the acoustic modes through convection and refraction effects, the next-order solutions must be constructed.

The $\mathcal{O}(M)$ acoustic equations derived from Eqs. (10–12) and (19) take the form

$$p_{2t} + u_{2x} + v_{2y} = -U(y)p_{1x} \tag{21}$$

$$u_{2t} + p_{2x} = -U(y)u_{1x} - v_1 U'(y) \tag{22}$$

$$v_{2t} + \frac{1}{h^2} p_{2y} = -U(y)v_{1x} \tag{23}$$

where density has been replaced by pressure according to Eqs. (20). Equations (16–18) can be combined with Eqs. (21–23) to find the nonhomogeneous wave equation for p_2,

$$p_{2tt} - \left(p_{2xx} + \frac{1}{h^2} p_{2yy}\right) = -2Ak^2\pi^2 U(y)\cos(k\pi t)\sin(k\pi x) \tag{24}$$

The forcing function on the right side is y-dependent and excites fully two-dimensional $\mathcal{O}(M)$ acoustic motion. The initial conditions for p_2 are simply [cf. Eqs. (13), (19), and (21)]

$$p_2(t = 0) = p_{2t}(t = 0) = 0 \tag{25}$$

The appropriate boundary conditions are derived by applying the results in Eqs. (16–23) to Eqs. (14) and (15), which gives

$$p_{2x}(x = 0) = -Ak\pi U(y)\cos(k\pi t)$$
$$p_{2x}(x = 1) = -(-1)^k Ak\pi U(y)\cos(k\pi t) \tag{26}$$

and

$$p_{2y}(y = 0) = p_{2y}(y = 1) = 0 \tag{27}$$

Equations (24–27) constitute a well-defined elementary two-dimensional hyperbolic system with a distributed source and axial boundary excitations. One notices that boundary conditions (26) are not compatible with Eq. (25) at $t = 0$. As a result, a pair of propagating discontinuities in p_{2x}, or weak discontinuities as described by Landau and Lifshitz,[7] are introduced at $x = 0$ and 1 at $t = 0$.

The solution to Eqs. (24–27) can be written as

$$\frac{p_2}{A} = -\cos(k\pi t)\sin(k\pi x)\sum_{n=0}^{\infty} \frac{\epsilon_n}{2} \tilde{U}_n \cos(n\pi y) + \sum_{m=0(m\neq k)}^{\infty}\sum_{n=0}^{\infty} \epsilon_m\epsilon_n \tilde{U}_n \Gamma_{mn}(k,t)\cos(m\pi x)\cos(n\pi y) \tag{28}$$

where ϵ_m and ϵ_n are the Neumann's number whose value equals 1 if the subscript is zero and 2 if it is a positive integer. The coefficients $\tilde{U}_n$ and Γ_{mn} are defined by

$$\tilde{U}_n = 2\int_0^1 U(y)\cos(n\pi y)\, dy \tag{29}$$

$$\Gamma_{mn} = \frac{[1-(-1)^{m+k}]k(m^2+k^2)}{2\pi(m^2+\bar{n}^2-k^2)(m^2-k^2)}\left[\frac{2k^2-\bar{n}^2}{m^2+k^2}\cos(k\pi t) - \cos\left(\sqrt{m^2+\bar{n}^2}\pi t\right)\right] \tag{30}$$

where $\bar{n} = n/h$. If $m^2 + \bar{n}^2 = k^2$, Γ_{mn} should be evaluated by taking the limit $m^2 + \bar{n}^2 - k^2 \to 0$ in Eq. (30), which yields $\mathcal{O}(t)$ amplification in p_2. It can be verified that Eq. (28) satisfies Eq. (24) as well as all initial and boundary conditions.

A more concise form of the solution is derived by combining the two terms in Eq. (28), which yields

$$\frac{p_2}{A} = \sum_{m=0(m\neq k)}^{\infty}\sum_{n=0}^{\infty} \epsilon_m\epsilon_n \tilde{U}_n \Theta_{mn}(k,t)\cos(m\pi x)\cos(n\pi y) \tag{31}$$

where

$$\Theta_{mn} = \begin{cases} \dfrac{[1-(-1)^{m+k}]k(m^2+k^2)}{2\pi(m^2+\bar{n}^2-k^2)(m^2-k^2)}\left[\cos(k\pi t) - \cos\left(\sqrt{m^2+\bar{n}^2}\pi t\right)\right], & m^2+\bar{n}^2 \neq k^2 \\ \dfrac{[1-(-1)^{m+k}](m^2+k^2)}{4(m^2-k^2)}\, t\sin(k\pi t), & m^2+\bar{n}^2 = k^2 \end{cases} \tag{32}$$

In the derivation of Eq. (31), $\sin(k\pi x)$ in Eq. (28) is expressed in terms of its Fourier cosine series whose derivative converges to zero instead of its true values at $x = 0$ and 1. As a result, the boundary conditions (26) are not satisfied by Eq. (31). However, Eq. (31) gives correct x derivatives elsewhere, including the immediate neighborhood of $x = 0$ and 1. The values of p_2 are not affected at all because the series given by Eq. (31) is uniformly convergent throughout the entire domain. Thus, one can justifiably use Eq. (31) to evaluate p_2 everywhere, and its first derivatives everywhere except at $x = 0$, 1, and at the locations of weak discontinuities where these derivatives are not defined.

The Fourier coefficients of the double series in Eq. (31) are proportional to $\tilde{U}_n$, which represents the shear flow effects, and vary with k and t. One observes from Eq. (32) that, for each nonresonant Fourier mode, the coefficient contains two harmonic functions of time with different frequencies. The first function, $\cos(k\pi t)$, has a frequency equal to that of the distributed forcing function in Eq. (24), or that of the imposed leading-order acoustic pressure. It describes the time depen-

dence of the Helmholtz mode of bulk oscillation with x- and y-dependent amplitudes.

The second cosine function in Eq. (32) is associated with wave phenomena. For each pair of m and $\bar{n}$, the product

$$P_{mn} = \cos\left(\sqrt{m^2 + \bar{n}^2}\pi t\right)\cos(m\pi x)\cos(n\pi y) \tag{33}$$

represents a two-dimensional oblique mode, which can be decomposed into four plane traveling waves:

$$\begin{aligned} P_{mn} = \frac{1}{4}\Big\{&\cos\left[\sqrt{m^2 + \bar{n}^2}\pi\left(t - z_{mn}^{+\,+}\right)\right] \\ &+ \cos\left[\sqrt{m^2 + \bar{n}^2}\pi\left(t - z_{mn}^{+\,-}\right)\right] \\ &+ \cos\left[\sqrt{m^2 + \bar{n}^2}\pi\left(t - z_{mn}^{-\,+}\right)\right] \\ &+ \cos\left[\sqrt{m^2 + \bar{n}^2}\pi\left(t - z_{mn}^{-\,-}\right)\right]\Big\} \end{aligned} \tag{34}$$

where

$$\begin{aligned} z_{mn}^{+\,+} &= \frac{mx + ny}{\sqrt{m^2 + \bar{n}^2}}, & z_{mn}^{+\,-} &= \frac{mx - ny}{\sqrt{m^2 + \bar{n}^2}} \\ z_{mn}^{-\,+} &= \frac{-mx + ny}{\sqrt{m^2 + \bar{n}^2}}, & z_{mn}^{-\,-} &= \frac{-mx - ny}{\sqrt{m^2 + \bar{n}^2}} \end{aligned} \tag{35}$$

are the paths taken by the traveling waves reflecting from duct walls and the axial acoustic reflectors. The wave paths are oblique in general. However, when either $m = 0$ or $n = 0$, the traveling waves are either transverse or axial, respectively, and the number of traveling waves reduces to two. Since Eq. (31) contains an infinite number of Fourier modes, one concludes that p_2 consists of infinite numbers of axial, transverse, and oblique standing waves, in addition to the bulk oscillation mentioned earlier. This is in sharp contrast to the results of the traveling wave study[5] where only a limited number of wave modes can propagate along a long duct. The multiple reflections of acoustic signals on the inserted acoustic reflectors create a more complex acoustic shear flow interaction response.

Although the asymptotic solution given by Eqs. (16), (19), (31), and (32) is derived primarily for processes occurring on the acoustic time scale of the duct, it is seen to be uniformly valid on the mean flow passage time scale $t \sim \mathcal{O}(M^{-1})$ as well, except for the resonant cases. Resonance occurs when the frequency of a transverse or oblique standing acoustic wave equals that of the forced vibration. It causes $\mathcal{O}(t)$ amplitude growth [cf. Eq. (32)] and invalidates the asymptotic expansion (19) as $t \sim \mathcal{O}(M^{-1})$. Comparing to the $\mathcal{O}(t^{1/2})$ resonant growth found for refraction induced traveling waves,[5] it is concluded that a trapped wave system produces faster growth rate for the resonant mode, owing to the effect of multiple axial reflections. In general, the asymptotic solution remains valid until $t \sim \mathcal{O}(M^{-2})$, the time required for the small nonlinear effects to accumulate, which leads to significant deformation of the leading-order waveform and possible formation of a weak shock in the confined geometry.[8]

A complete solution should include the thin acoustic boundary layers adjacent to the duct walls. An approach identical to that used in Ref. 5 can be applied to reveal the structure of the transport-dominated layers. A preliminary analysis shows a basically uniform acoustic pressure distribution across the layer, whose thickness is proportional to the ratio of the fluid kinematic viscosity to the mode number k of the basic core pressure disturbance. A multitude of velocity standing modes induced by the core acoustic flow are strongly damped by viscous and thermal diffusion to satisfy no-slip and appropriate thermal boundary conditions.[5,9] Since no fundamentally new discoveries are expected from a detailed analysis, it is not pursued here.

IV. Example Calculations and Discussion

A. Acoustic Convection and Refraction

The effect of a sheared mean flow on acoustic processes can be more clearly elucidated by rewriting Eq. (31) as $p_2 = p_{2C} + p_{2R}$, where

$$p_{2C} = A\tilde{U}_0 \sum_{m=0(m\neq k)}^{\infty} \epsilon_m \Theta_{m0}(k,t)\cos(m\pi x) \tag{36}$$

$$p_{2R} = 2A \sum_{m=0(m\neq k)}^{\infty} \sum_{n=1}^{\infty} \epsilon_n \tilde{U}_n \Theta_{mn}(k,t)\cos(m\pi x)\cos(n\pi y) \tag{37}$$

The first component of p_2, p_{2C}, contains all of the $n = 0$ Fourier modes. It is directly proportional to the shear flow velocity averaged across the duct ($\tilde{U}_0/2$) [cf. Eq. (29)] and is the correction to the basic acoustic pressure [Eq. (16)] that would arise in a pure slug flow. This effect, henceforth referred to as the bulk convection effect, is accountable for the axial standing wave disturbances and the y-independent part of the bulk oscillations in p_2. The magnitude of bulk convection increases with the average shear flow velocity and the mode number k of the basic acoustic disturbance, as can be shown from Eq. (32). When Mp_{2C} is superimposed on the basic acoustic pressure p_1, the total acoustic pressure remains one-dimensional, although its waveform is slightly distorted in the axial direction by a time-dependent periodic function.

The quantity p_{2R} in Eq. (37) arises from convection of the basic axial acoustic disturbance at the local differential velocity $U(y) - \tilde{U}_0/2$. Thus, p_{2R} is associated with refraction of the axially distributed solution p_1 in Eq. (16) by the shear flow. It is seen to be intricately related to the specific shear flow velocity profile through the Fourier coefficients $\tilde{U}_n$. Both transverse and oblique standing acoustic waves are present, and amplitude amplification of certain modes is possible as a result of resonance phenomena. The p_{2R} solution also includes bulk oscillations with y-dependent amplitudes, as mentioned in Sec. III.

The general features of the acoustic field described by Eqs. (16), (31), and (32) can be revealed graphically by evaluating these expressions numerically. In the subsequent calculations, each Fourier summation is carried out up to the 50th term, with a truncation error of less than 10^{-3} based on comparisons of the results with those from summations of 100 or more terms. Three types of shear flows $U(y)$, as well as different combinations of mode number k and duct aspect ratio h, are employed to generate representative results. The amplitude of the initial disturbance A is kept at unity since both p_1 and p_2 exhibit the same simple proportionality to it. Results are presented in terms of p_{2C} and p_{2R}, mentioned earlier, for easier physical interpretation.

Figs. 2a-c display the time variations of the three acoustic pressure components on the duct wall ($y = 1$) at axial locations $x = 0$, ¼, and ½, respectively. The wave field is generated by the relaxation of the initial velocity disturbance $\hat{u} = \sin(\pi x)$ ($k = 1$) in a fully developed laminar flowfield described by $U = 1 - y^2$. The duct section considered has equal length and width, so that $h = ½$. In each figure, the solid line denotes the basic acoustic pressure p_1, as calculated from Eq. (16). The amplitude of its oscillation is seen to decrease from maximum at the antinode $x = 0$ (cf. Fig. 2a) to zero at the nodal plane $x = ½$ (cf. Fig. 2c). The long- and short-dashed lines represent the bulk convective correction p_{2C} and the refractive correction p_{2R}, calculated from Eqs. (36) and (37), respectively. The former is a y-independent, periodic function of time whose amplitude and structure vary with axial position x, as observed from the figures. The time response of p_{2R} depends on both spatial coordinates and exhibits nonperiodic, irregular oscillatory behavior, as a result of the superposition of signals with noncommensurate frequencies arising from transverse and oblique standing modes as well as the bulk modes. The slope discontinuities on both p_{2C} and p_{2R} curves denote the

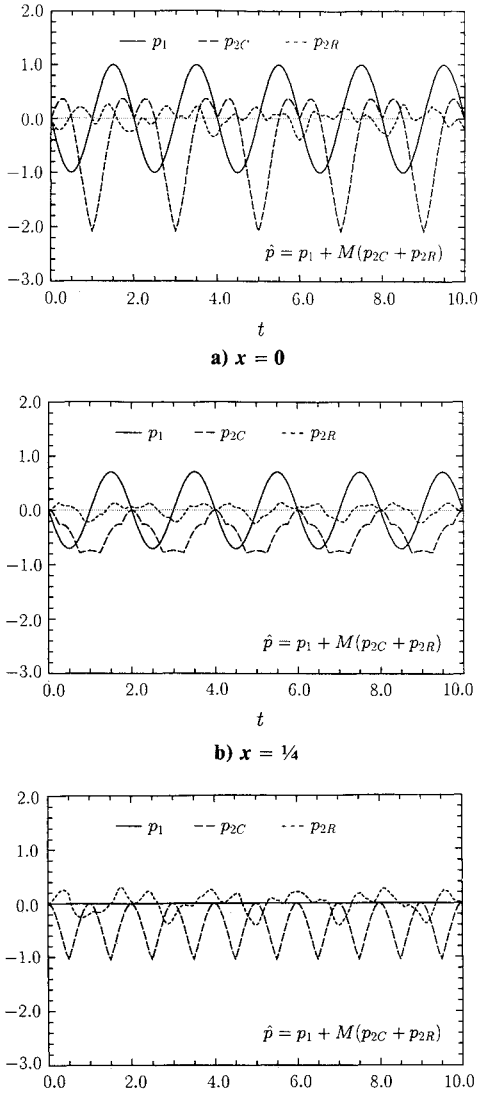

Fig. 2 Time variations of p_1, p_{2C}, and p_{2R}, as calculated from Eqs. (16), (36), and (37), respectively, on the duct wall $y = 1$ at three axial locations; the acoustic field is generated by the relaxation of an initial disturbance $\hat{u}(t = 0) = \sin(\pi x)$ in a laminar duct flow $U = 1 - y^2$; the duct aspect ratio $h = ½$.

passage of the weak discontinuities created by the initial jump in p_{2x} [cf. Eqs. (26)]. The curves in Figs. 2a–c are plotted up to $t = 10$, at which the mean flow completes one passage through the duct section if $M = 0.1$, and an axial acoustic signal is reflected 10 times on the left and right boundaries. Longer-time calculations produce similar irregular patterns for p_{2R} while p_1 and p_{2C} continue their periodic variations. It is particularly interesting to notice in Fig. 2c that, although the basic acoustic pressure p_1 vanishes, the total acoustic pressure $\hat{p} = p_1 + M(p_{2C} + p_{2R})$ is nonzero because a mean flowfield with shear is present.

The two-dimensional structure of the acoustic pressure due to refraction (p_{2R}) is illustrated in Figs. 3a and 3b, which depict p_{2R} distributions in the duct for an acoustic shear flow system characterized by $k = 3$, $h = 1/6$, and $U = 1 - y^2$, at $t = ⅝$ and 7, respectively. The two snapshots are more than six acoustic time units apart, and thus do not reflect the waveform evolution process, which occurs on a much shorter time scale. The lines of sharp slope changes associated with the propagating weak discontinuities are obvious on the p_{2R} surfaces. The absolute magnitude of the refraction effect is small because p_{2R} must be multiplied by M.

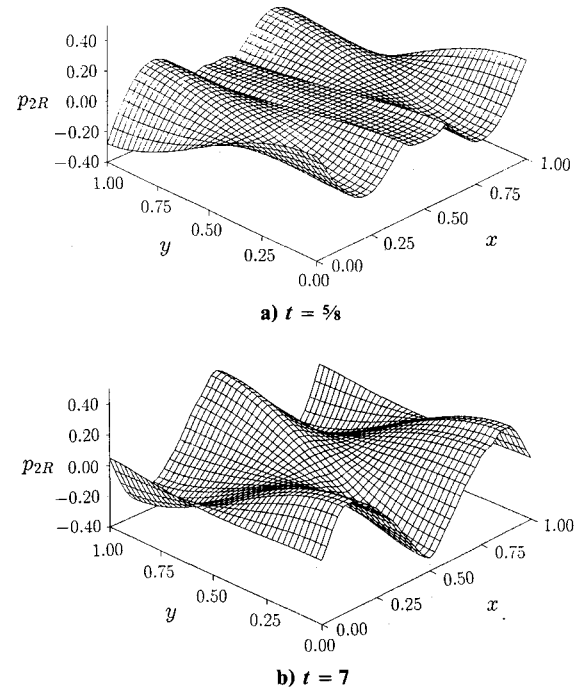

Fig. 3 Distribution of second-order acoustic pressure due to refraction (p_{2R}) in the duct section, as calculated from Eq. (37); the refraction effects are generated as the initial acoustic disturbance $\hat{u}(t = 0) = \sin(3\pi x)$ relaxes in the shear flowfield $U = 1 - y^2$; the duct aspect ratio $h = 1/6$.

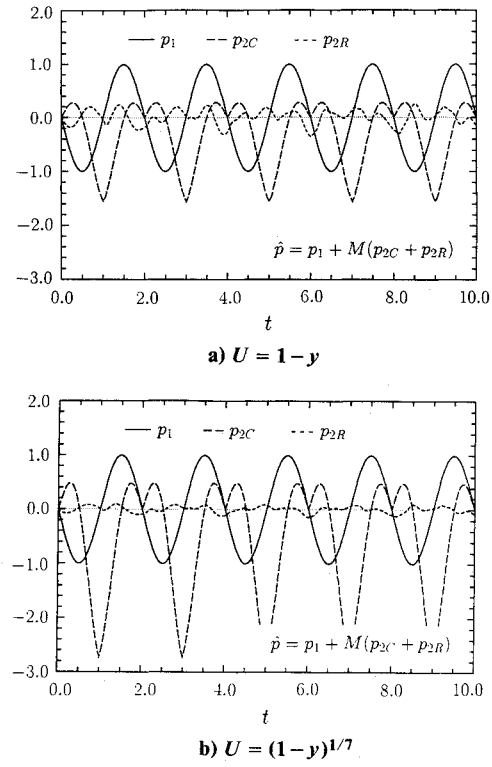

Fig. 4 Time variations of p_1, p_{2C}, and p_{2R} at $x = 0$, $y = 1$, generated by the relaxation of the initial disturbance $\hat{u}(t = 0) = \sin(\pi x)$ in shear flowfields; the duct aspect ratio $h = ½$.

B. Effect of Mean Flow Type

Figures 4a and 4b illustrate the time history of p_1, p_{2C}, and p_{2R} at $x = 0$, $y = 1$ under the same conditions as in Fig. 2a, except for different shear flow velocity types. In Fig. 4a, $U = 1 - y$, corresponding to a fully developed Couette flow in

the half duct considered. The profile $U=(1-y)^{1/7}$ is used to find the results shown in Fig. 4b. It is easily observed from Figs. 2a, 4a, and 4b that the shear flow described by the one-seventh power law generates the largest bulk convection effect p_{2C} because it has the largest average velocity. Analogously, the parabolic flow creates a larger bulk convection effect than the linear flow. The refraction effects for the linear and parabolic flow types are of comparable magnitude. The one-seventh power law flow generates the smallest acoustic refraction because the velocity gradient is relatively small in most of the core flow region. The large velocity gradient is concentrated within a thin layer near the wall that is too narrow to promote acoustic refraction on a global scale in the core.

The refraction induced acoustic pressure fluctuations at specified locations are plotted alone in Figs. 5a and 5b for the parabolic and one-seventh power mean flow types, under conditions $k=1$ and $h=\frac{1}{2}$. The solid and dashed lines, representing p_{2R} at an axial position $x=\frac{1}{2}$ on the center plane ($y=0$) and duct wall ($y=1$), respectively, resemble each other but are completely out of phase, implying the relative importance of refraction in the duct. It is strikingly noteworthy that superpositions of various linear wave structures resulting from shear flow interactions with a simple axial disturbance can produce fairly irregular pressure signals, which might be mistakenly attributed to nonlinear phenomena had the data been collected from numerical or experimental investigations. The shear velocity described by the one-seventh power law is again shown to generate smaller p_{2R} than the other case.

C. Effect of Mode Number and Duct Aspect Ratio

The earlier traveling wave study[5] suggests that the magnitude of acoustic refraction phenomena is controlled by, among other parameters, the ratio of the wavelength to the duct width. For a duct of fixed width, higher frequency waves induce a relatively larger refraction effect. In the present analysis, due to the finite axial length of the flow geometry, the relationship between p_{2R} and the parameters k and h is more complex [cf. Eqs. (37) and (32)]. Nonetheless, numerical evaluations show that when k is away from resonant frequencies of the duct the same trend is apparent.

The nonresonant p_{2R} curves in Figs. 6a and 6b are plotted at $x=0$, $y=0$ and 1 using the same shear flow velocity $U=1-y^2$. The k and h values are selected such that, while k increases from 1 in Fig. 6a to 3 in Fig. 6b, the aspect ratio h decreases in proportion so that the wavelength-to-duct-width ratio remains constant. As expected, the refraction induced pressure fluctuations in the two figures are comparable in magnitude, and the frequency of fluctuation increases with k. The p_{2R} signals are all fairly irregular. The location $x=0$ is chosen in Figs. 6a and 6b because it corresponds to the antinode for p_1, where p_{2R} curves are of typical magnitude for both cases. At other x positions, p_{2R} fluctuates in a similar manner with different rates and amplitudes (see, for example, Fig. 5a).

Figure 7 shows a near resonant case that results in a long period beat pattern. Here, $k=4$, $h=\frac{1}{4}$, so that, for $m=1$ and $n=1$, $m^2+\bar{n}^2=17$ while $k^2=16$. The p_{2R} curves are plotted at $x=\frac{1}{8}$, $y=0$ and 1, for $U=1-y^2$. Beats of even longer periods and larger maximum amplitudes can occur at suitable parameter combinations. If the numerical evaluation of the solution had been limited to times less than half the beat period, the result could have been erroneously interpreted as an amplified mode.

Fully resonant solution behavior is shown in Figs. 8a and 8b, where p_{2R} on the duct wall is depicted at $x=1/10$ and $x=\frac{1}{2}$, respectively, for $U=1-y^2$ and $k=5$. In Fig. 8a, $h=1/5$, so that the transverse mode ($m=0$, $n=1$) is amplified. Figure 8b corresponds to $h=1/\sqrt{21}$, which promotes the amplification of an oblique mode ($m=2$, $n=1$). One may observe beat patterns superimposed on the long-time growth arising from the interference by near-resonant modes.

The considerable enhancement of the refractive acoustic pressure by resonance requires a new asymptotic solution on the flow time scale $t\sim\mathcal{O}(M^{-1})$ to accommodate refraction phenomena in the leading-order acoustics. Likewise, when

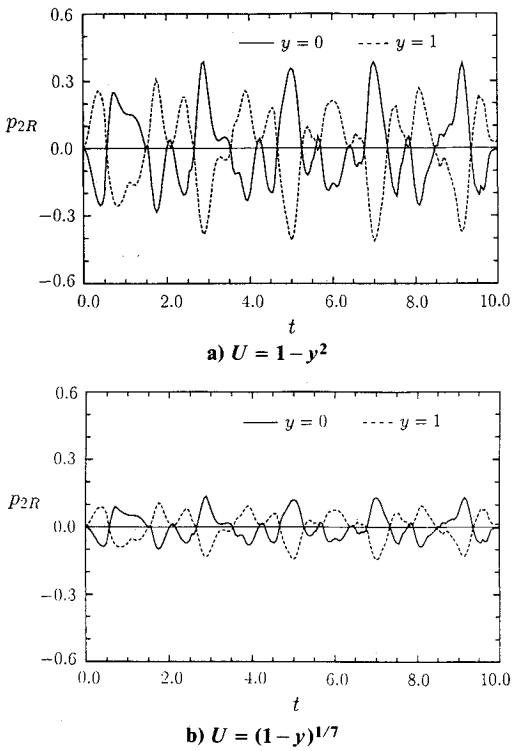

a) $U=1-y^2$

b) $U=(1-y)^{1/7}$

Fig. 5 Time variations of refractive acoustic pressure p_{2R} as calculated from Eq. (37), at locations $x=\frac{1}{2}$, $y=0$ and 1. The refraction effects are generated by the relaxation of the initial acoustic disturbance $\hat{u}(t=0)=\sin(\pi x)$ in shear flows; the duct aspect ratio $h=\frac{1}{2}$.

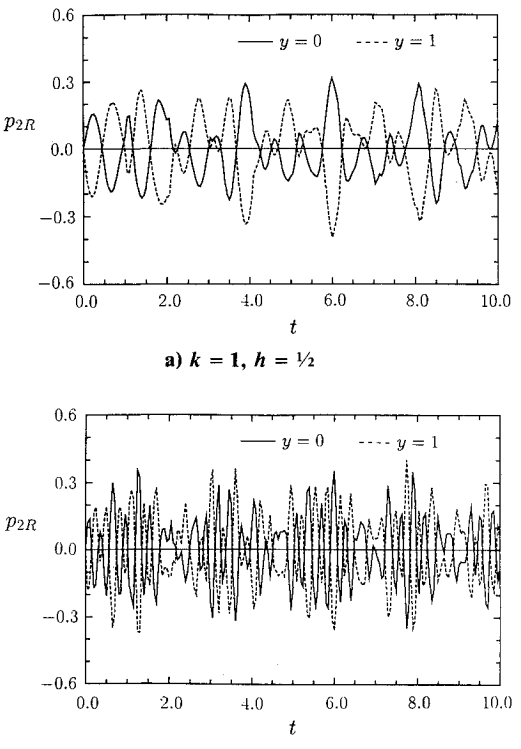

a) $k=1$, $h=\frac{1}{2}$

b) $k=3$, $h=1/6$

Fig. 6 Time variations of refractive acoustic pressure p_{2R} at locations $x=0$, $y=0$ and 1, generated as the initial acoustic disturbance $\hat{u}(t=0)=\sin(k\pi x)$ relaxes in the shear flowfield $U=1-y^2$.

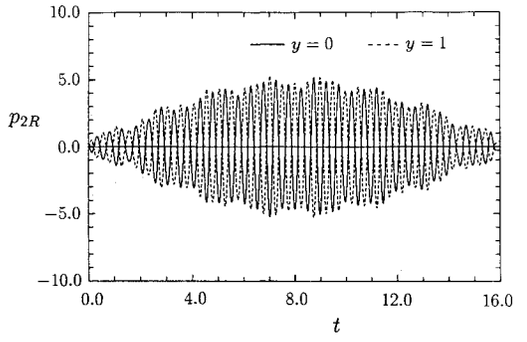

Fig. 7 Near-resonant variations of refractive acoustic pressure p_{2R} with time at locations $x = 1/8$, $y = 0$ and 1, as the initial acoustic disturbance $\hat{u}(t = 0) = \sin(4\pi x)$ relaxes in the shear flowfield $U = 1 - y^2$; the duct aspect ratio $h = 1/4$.

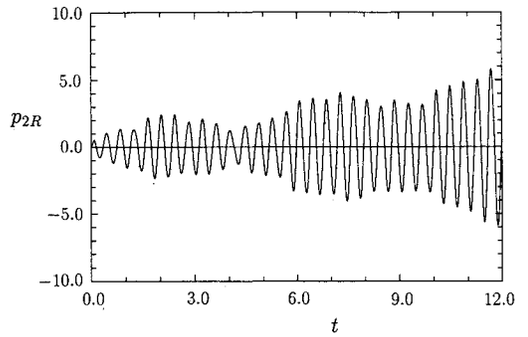

a) $h = 1/5$, $x = 1/10$

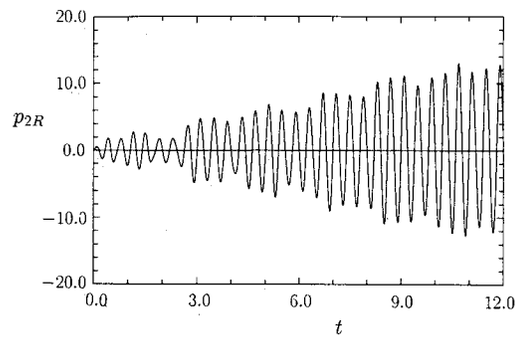

b) $h = 1/\sqrt{21}$, $x = 1/2$

Fig. 8 Resonant amplifications of refractive acoustic pressure p_{2R} on the duct wall ($y = 1$), at specified axial locations, as the initial acoustic disturbance $\hat{u}(t = 0) = \sin(5\pi x)$ relaxes in the shear flowfield $U = 1 - y^2$.

certain modes oscillate at near-resonant frequencies of the system, or when the mode number k becomes large and the aspect ratio h small, so that $Mp_2 \sim \mathcal{O}(p_1)$, a new theory needs to be developed.

D. Inferences About Solid Rocket Engine Acoustics

Solid rocket combustion chamber dimensions are usually associated with radius-to-length ratios less than or equal to $\mathcal{O}(1)$. Experimental observations suggest that the first few acoustic modes, especially the $k = 1$ mode, are most frequently encountered in rocket chambers. Based on this analysis, the convection and refraction induced acoustic pressure correction terms are at most $\mathcal{O}(M)$ relative to the leading-order acoustic pressure, or $\mathcal{O}(M^3)$ relative to the overall pressure. Although resonance in p_{2R} significantly magnifies the acoustic refraction, it occurs rarely for low k modes. In fact, the resonant condition $m^2 + (n/h)^2 = k^2$ indicates that there can be no resonant modes if $kh < 1$, which is likely to be the case given the sizes of k and h mentioned earlier. Thus, a mean flow with $M = 0.1$ causes at most $\mathcal{O}(10^{-1})$ changes in acoustic pressure, or $\mathcal{O}(10^{-3})$ changes in total pressure. The nonlinear effects, represented by quadratic terms in the convective operators and responsible for acoustic streaming, are $\mathcal{O}(10^{-1})$ smaller. They are of no importance on the time scale considered here and accumulate only on the longer time scale $t \sim \mathcal{O}(10^2)$.

The resonant phenomenon discussed earlier appears in second-order acoustic quantities only and is excited by interactions with a sheared mean flow. It should be distinguished from the more powerful resonance of leading-order acoustic pressure in a rocket engine configuration, often associated with excitations arising from chemical heat release, which is beyond the scope of this paper.

V. Summary

In this paper, a mathematical model is established to study the interaction between a low Mach number parallel shear flow and an axially distributed acoustic disturbance trapped in a section of a planar duct. The solution development is based on asymptotic expansions defined for the small mean flow Mach number limit ($M \to 0$). The Fourier-series-based analytical solution in terms of standing modes gives explicit modal response of the acoustic shear flow interactions. The major conclusions are the following:

1) Bulk (slug flow) convection induces purely axial standing acoustic waves and y-independent bulk oscillations at the frequency of the imposed initial disturbance. The magnitude of the bulk convection effect increases with the average shear flow velocity and the mode number k of the leading-order acoustic pressure.

2) Refraction generates purely transverse and oblique standing waves as well as bulk oscillations with both x- and y-dependent amplitudes. The magnitude of refraction increases with the shear flow velocity gradient, the duct-width-to-length ratio h and the mode number k of the leading-order acoustic pressure. The refraction size also increases if the frequencies of the induced acoustic modes become close to the resonant frequency.

3) Combination of the effects just mentioned gives irregular pressure signals at given positions in the duct. They are of $\mathcal{O}(M)$ relative to the imposed leading-order acoustic pressure.

4) Axial wave reflections cause faster resonant growth of acoustic refraction. Resonance does not occur for $hk < 1$.

5) Refraction effects are very small in both traveling and standing wave model studies in the parameter ranges of solid rocket engines.

The primary point is that quite elementary disturbances can evolve into surprisingly complex wave structures as a result of refraction effects, although these effects are small in the parameter ranges of solid rocket engines. This simplified analysis gives insight into the acoustic modal interactions with the shear flow, which have not been extracted from computational data in past studies. In fact, there appears to be a specific need to develop data anlysis tools that are capable of using grid point flow data to determine the propagating wave patterns present in an acoustically excited shear flow.

Acknowledgment

This work was supported by the Air Force Office of Scientific Research through Grant AFOSR 89-0023.

References

[1]Pridmore-Brown, D. C., "Sound Propagation in a Fluid Flowing Through an Attenuating Duct," *Journal of Fluid Mechanics*, Vol. 4, 1958, pp. 393–406.

[2]Mungur, P., and Gladwell, G. M. L., "Acoustic Wave Propagation in a Sheared Fluid," *Journal of Sound and Vibration*, Vol. 9, No. 1, 1969, pp. 28–48.

[3]Hersh, A. S., and Catton, I., "Effect of Shear Flow on Sound Propagation in Rectangular Ducts," *Journal of the Acoustical Society of America,* Vol. 50, No. 3, 1971, pp. 992–1003.

[4]Baum, J. D., and Levine, J. N., "Numerical Investigation of Acoustic Refraction," *AIAA Journal,* Vol. 25, No. 12, 1987, pp. 1577–1586.

[5]Wang, M., and Kassoy, D. R., "Transient Acoustic Processes in a Low Mach Number Shear Flow," *Journal of Fluid Mechanics,* Vol. 238, 1992, pp. 509–536.

[6]Price, E. W., "Experimental Observations of Combusion Instability," *Fundamentals of Solid-Propellant Combustion,* edited by K. Kuo and M. Summerfield, Vol. 90, Progress in Astronautics and Aeronautics, AIAA, New York, 1984, pp. 733–790.

[7]Landau, L. D., and Lifshitz, E. M., *Fluid Mechanics,* Pergamon Press, London, 1959, pp. 344–346.

[8]Wang, M., and Kassoy, D. R., "Evolution of Weakly Nonlinear Waves in a Cylinder with a Movable Piston," *Journal of Fluid Mechanics,* Vol. 221, 1990, pp. 27–52.

[9]Lighthill, M. J., "Acoustic Streaming," *Journal of Sound and Vibration,* Vol. 61, No. 3, 1978, pp. 391–418.